Anomalous $h/2e$ Periodicity and Majorana Zero Modes in Chiral Josephson Junctions

Zi-Ting Sun[1,*], Jin-Xin Hu,[1,*] Ying-Ming Xie[2,†] and K. T. Law[1,‡]

[1]*Department of Physics, Hong Kong University of Science and Technology, Clear Water Bay, Hong Kong, China*
[2]*RIKEN Center for Emergent Matter Science (CEMS), Wako, Saitama 351-0198, Japan*

Recent experiments reported that quantum Hall chiral edge state-mediated Josephson junctions (chiral Josephson junctions) could exhibit Fraunhofer oscillations with a periodicity of either h/e [Vignaud *et al.*, Nature (London) **624**, 545 (2023)] or $h/2e$ [Amet *et al.*, Science **352**, 966 (2016)]. While the h/e-periodic component of the supercurrent had been anticipated theoretically before, the emergence of the $h/2e$ periodicity is still not fully understood. In this Letter, we systematically study the Fraunhofer oscillations of chiral Josephson junctions. In chiral Josephson junctions, the chiral edge states coupled to the superconductors become chiral Andreev edge states. We find that in short junctions, the coupling of the chiral Andreev edge states can trigger the $h/2e$-magnetic flux periodicity. Our theory resolves the important puzzle concerning the appearance of the $h/2e$ periodicity in chiral Josephson junctions. Furthermore, we explain that when the chiral Andreev edge states couple, a pair of localized Majorana zero modes appear at the ends of the Josephson junction, which are robust and independent of the phase difference between the two superconductors. As the $h/2e$ periodicity and the Majorana zero modes have the same physical origin in the wide junction limit, the Fraunhofer oscillation period could be useful in identifying the regime with Majorana zero modes.

Introduction—The topological boundary state-superconductor hybrids are promising platforms for realizing Majorana zero modes (MZMs) and topological quantum computation [1–8]. In the past decade, Josephson junctions with supercurrents mediated by edge states had been achieved in various topological systems, such as in quantum Hall insulators [9–15], the quantum spin Hall insulator HgTe/HgCdTe quantum wells [16], and the higher order topological insulators [17–19]. In the experiments, the Fraunhofer pattern that measures the critical currents as a function of external magnetic flux was widely used to identify edge state-mediated Josephson junctions. A prominent feature of edge state-mediated Josephson junctions is the superconducting quantum interference device (SQUID) like oscillations in the Fraunhofer patterns [16,20–22] as illustrated in the right panels of Fig. 1.

Josephson junctions with chiral edge states (CESs) as the weak links are particularly interesting [23–26]. In these chiral Josephson junctions, the supercurrents are medicated by chiral edge states. It was anticipated by theories that chiral Josephson junctions exhibit $2\Phi_0 = h/e$ periodicity in the Fraunhofer patterns, where $\Phi_0 = h/2e$ is the magnetic flux quantum [23,26–30]. As depicted in
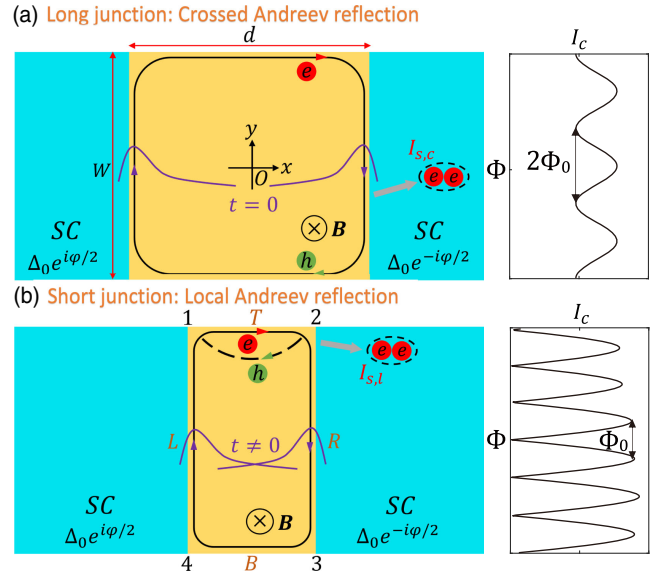
FIG. 1. Origins of $2\Phi_0$ and Φ_0 periodicity in chiral Josephson junctions. (a) In the long junction, the crossed Andreev reflection processes dominate. Namely, an electron e from the top edge (T) is reflected as a hole h in the bottom edge (B). This results in a Cooper pair e-e entering the superconductor (SC). The critical Josephson current I_c as a function of magnetic flux Φ has a period of $2\Phi_0$ (right panel). The cross circle denotes out of plane magnetic field $\boldsymbol{B}$. (b) In the short junction, the wave functions (purple lines) of the left (L) and right (R) edge state (L) are coupled, where the supercurrent is mainly mediated by the local Andreev reflections, which results in a Fraunhofer pattern with a period of Φ_0 instead (right panel).

---
[*]These authors contributed equally to this work.
[†]Contact author: yxieai@connect.ust.hk
[‡]Contact author: phlaw@ust.hk

Fig. 1(a), due to the chiral nature of the CESs, in long junctions the Andreev reflections can happen only when an electron from the top (T) edge hits the CES/superconductor interface and is reflected as a hole along the bottom (B) edge [T and B label the edges as in Fig. 1(b)]. Such Andreev reflections involving two CESs in a single tunneling process are crossed Andreev reflections. The $2\Phi_0$-period of the Fraunhofer oscillations is twice the period of conventional SQUIDs involving Cooper pair interference and is experimentally observed very recently (Vignaud *et al.* [15]). However, in another experiment by Amet *et al.* [11], Φ_0 periodicity was observed. Other previous theoretical works reported in Refs. [28] and [29] noticed such inconsistency between theories and the experiments, but it remains a puzzle how the Φ_0 periodicity emerges in a chiral Josephson junction [11]. Therefore, a theory that clarifies the Fraunhofer pattern in chiral Josephson junctions is highly desirable at the current stage.

In this Letter, we revisit the Fraunhofer patterns in chiral Josephson junctions. Unlike previous theories, we take into account the possible hybridization between the chiral edge states (or more precisely, the chiral Andreev edge states introduced later) along the two quantum (or anomalous) Hall or superconductor interfaces (see the left panels of Fig. 1). Using an edge-channel model as well as a lattice model, we unambiguously show that such hybridization would result in a crossover of the period in Fraunhofer oscillations from $2\Phi_0$ to Φ_0 as the junction length decreases. Specifically, we find that the supercurrents originated from crossed Andreev reflections between two separated edges [see Fig. 1(a)] give rise to $2\Phi_0$ oscillations, while the supercurrents that originated from local Andreev reflections [see Fig. 1(b)] exhibit Φ_0 oscillations. Importantly, we demonstrate that in the Φ_0 periodicity regime, robust MZMs appear at the Josephson junction without fine-tunings. Our theory suggests that short superconductor or quantum anomalous Hall insulator (QAHI) or superconductor Josephson junctions are promising platforms for realizing MZMs (Fig. 3).

Edge-channel model—We first construct an edge-channel model to capture the low-energy physics of Josephson junctions with CESs in the weak link as depicted in Fig. 1. This model is applicable to describe Josephson junctions with a quantum Hall or a QAHI weak link. In this model, the two superconductors have a bulk pairing potential Δ_0 and a phase difference φ. The electrons of the CESs propagate in a clockwise direction. Thus the model Hamiltonian reads

$$H = \sum_{\gamma} \int d\boldsymbol{r}\, \Psi_{\gamma}^{\dagger}(\boldsymbol{r}) H_{\gamma}^{\mathrm{BdG}}(\boldsymbol{r}) \Psi_{\gamma}(\boldsymbol{r}), \quad (1)$$

where γ labels the left or right (L/R) and top or bottom (T/B) edges. The Nambu basis vector $\Psi_{\gamma}(\boldsymbol{r}) = [\psi_{\uparrow\gamma}(\boldsymbol{r}), \psi_{\downarrow\gamma}^{\dagger}(\boldsymbol{r})]^T$, where $\psi_{s\gamma}(\boldsymbol{r})$ is an annihilation operator

for an electron with spin s at γ edge at position $\boldsymbol{r}$. The Bogoliubo–de Gennes (BdG) Hamiltonian reads

$$H_{\gamma}^{\mathrm{BdG}}(\boldsymbol{r}) = H_{0,\gamma}^{\mathrm{BdG}}(\boldsymbol{r}) + H_{1}^{\mathrm{BdG}}(\boldsymbol{r}). \quad (2)$$

Here, $H_{0,\gamma}^{\mathrm{BdG}}(\boldsymbol{r})$ is the propagating Hamiltonian of four edges in Fig. 1(a), while $H_{1}^{\mathrm{BdG}}(\boldsymbol{r})$ characterize the coupling between the left and the right CESs [Fig. 1(b)]. The exact form of $H_{1}^{\mathrm{BdG}}(\boldsymbol{r})$ is not a concern here. As it is shown later, $H_{1}^{\mathrm{BdG}}(\boldsymbol{r})$ is responsible for giving rise to the $h/2e$ periodicity in the Fraunhofer oscillations. In the presence of an out-of-plane magnetic field, the propagating Hamiltonian yields

$$H_{0,\gamma}^{\mathrm{BdG}} = \begin{pmatrix} \boldsymbol{v}_{\gamma} \cdot (\hat{\boldsymbol{p}} + e\boldsymbol{A}) - \mu_{\gamma} & \Delta_{\gamma} e^{i\chi_{\gamma}\frac{\varphi}{2}} \\ \Delta_{\gamma} e^{-i\chi_{\gamma}\frac{\varphi}{2}} & \boldsymbol{v}_{\gamma} \cdot (\hat{\boldsymbol{p}} - e\boldsymbol{A}) + \mu_{\gamma} \end{pmatrix}. \quad (3)$$

Here, the momentum operator is $\hat{\boldsymbol{p}} = -i\hbar\nabla$, Δ_{γ} is the effective pairing potential ($\Delta_{\gamma=T/B} = 0$, $\Delta_{\gamma=L/R} = \Delta$), μ_{γ} is the chemical potential ($\mu_{\gamma=L/R} = \mu'$, $\mu_{\gamma=T/B} = \mu$), $\boldsymbol{v}_{\gamma}$ denotes the Fermi velocity of edge states ($\boldsymbol{v}_{\gamma=T/B} = (\chi_{\gamma}v_F, 0)$, $\boldsymbol{v}_{\gamma=L/R} = (0, \chi_{\gamma}v_s)$ with $\chi_{L/R} = \chi_{T/B} = \pm 1$), v_F is the bare velocity of CESs, and v_s is the renormalized Fermi velocity. Note that the chemical potential μ' of the left and right edges is affected by the superconductor, which can be different from the chemical potential μ of the top and bottom edges [14]. Moreover, because of the proximity effects, in which the electrons enter the superconductors virtually, v_s would be approximately renormalized as $v_s \approx v_F/(1 + g/\Delta_0)$ and the proximity pairing potential $\Delta \approx g\Delta_0/(g + \Delta_0)$ with g as an effective coupling strength [15,29]. The Landau gauge $\boldsymbol{A} = -yB\hat{\boldsymbol{x}}$ captures the effects of a magnetic field with strength B.

Possible Andreev reflection processes in short and long junctions—Before evaluating the supercurrent mediated by the CESs in Fig. 1, we first analyze the possible Andreev reflection processes. Such processes are significantly different in short and long junction limits. In the long junction limit where the coupling Hamiltonian $H_{1}^{\mathrm{BdG}}(\boldsymbol{r})$ is negligible, the electrons and holes on the CESs propagate circularly along the edges. It is worth noting that the electrons and holes propagate in the same direction on a CES. As a result, for an Andreev reflection process, an incoming electron at the top edge can only be reflected as a hole at the bottom edge [see Fig. 1(a)]. Such crossed Andreev reflections result in a Cooper pair tunneling from the top edge to the superconductor on the right, leading to a supercurrent denoted by $I_{s,c}$. On the other hand, in the short junction case, an additional Andreev reflection path could appear. As schematically shown in Fig. 1(b), an incoming electron at the top edge can be directly reflected as a hole to the left edge because of the finite coupling between the left and right CESs. Such local Andreev reflections at one edge give rise to a supercurrent denoted by $I_{s,l}$. In the following

section, by using the scattering matrix method [31], we demonstrate that $I_{s,l}$ and $I_{s,c}$ have periods Φ_0 and $2\Phi_0$, respectively.

Scattering matrix for chiral Josephson junctions—To derive the scattering matrix, we first analyze the scattering modes given by the eigenstates of $H_{0,\gamma}^{\text{BdG}}$. Specifically, the scattering modes behave as plane waves of pure electrons and holes on the top and bottom edges. Explicitly, on the left and right edges, the scattering modes are superpositions of electrons and holes, yielding

$$\Psi_{e\gamma}^S = \zeta_{e\gamma} e^{ik_{s,e,\gamma}y}, \qquad \Psi_{h\gamma}^S = \zeta_{h\gamma} e^{ik_{s,h,\gamma}y} \qquad (4)$$

with the wave vector $k_{s,e/h,\gamma} = \left(\epsilon \pm \sqrt{\Delta^2 + \mu'^2}\right)/\chi_\gamma \hbar v_s$, ϵ is the energy, $e(h)$ represents the electron (hole)-like state. $\zeta_{e\gamma} = (e^{i\chi_\gamma\varphi/2}, -e^{-\beta})_\gamma^T$, $\zeta_{h\gamma} = (e^{-\beta}, e^{-i\chi_\gamma\varphi/2})_\gamma^T$, with $\beta = \text{arcsinh}(\mu'/\Delta)$. The subscript γ and χ_γ are defined in the same way as in the BdG Hamiltonian. These chiral modes were called chiral Andreev edge states (CAES) in previous experiments [32,33]. As will be shown later, the CAES are essential for realizing MZMs in the chiral Josephson junctions.

However, the CAES become nonchiral due to the hybridization effect of the wave functions when the junction length d is comparable with the localization length ξ_d of the CAES, i.e., the coupling Hamiltonian H_1^{BdG} becomes essential. In this case, the left and right edges are coupled, and we can rewrite the two scattering modes

$$\Psi_{\alpha+}^S = \left[r_{\alpha,LL}\zeta_{\alpha L} + t_{\alpha,LR}\zeta_{\alpha R}\right] e^{ik_{s,\alpha,+}y},$$
$$\Psi_{\alpha-}^S = \left[r_{\alpha,RR}\zeta_{\alpha R} + t_{\alpha,RL}\zeta_{\alpha L}\right] e^{ik_{s,\alpha,-}y}, \qquad (5)$$

where $\pm$ labels the propagating direction, $\alpha = e/h$, and $\chi_{e/h} = \pm 1$. We assume the dispersion relation of the scattering modes does not change as an approximation, i.e., $k_{s,\alpha,\pm} = \pm\left(\epsilon + \chi_\alpha\sqrt{\Delta^2 + \mu'^2}\right)/\hbar v_s$. The overlap of the left and right edges is characterized by $t_{\alpha,LR(RL)} = e^{-(d/\xi_d)\mp i\chi_\alpha\pi(\Phi/\Phi_0)(y/W)}$, which is dressed by Peierls substitution and is exponentially suppressed when d/ξ_d increases. Here, the magnetic flux $\Phi = BdW$ with W as the junction width. Note that the unitary condition requires $|r_{\alpha,\gamma\gamma}|^2 + |t_{\alpha,\gamma\gamma'}|^2 = 1$ and $r_{\alpha,\gamma\gamma} = \sqrt{1 - \exp(-2d/\xi_d)}$ is assumed.

Origin of h/e and $h/2e$ periodicity—The flux-dependent Josephson current through the junction is related to the scattering matrix by [34]

$$I_s(\varphi, \Phi) = -\frac{2ek_BT}{\hbar}\frac{d}{d\varphi}\sum_{n=0}^{\infty} \ln\det\left[1 - \mathcal{S}_A(i\omega_n)\mathcal{S}_N(i\omega_n)\right],$$
$$(6)$$

where $\omega_n = (2n+1)\pi k_B T$ are fermionic Matsubara frequencies, T is the temperature. The scattering matrix

S_N describes the normal transimission from 1 to 2 (3 to 4) at the top (bottom) edge, while the scattering matrix S_A captures all possible Andreev reflection processes that scatter an incoming scattering state at 2 or 4 into an outgoing state at 3 or 1 through the left and right edges [see Fig. 1(b)]. The explicit forms of S_N and S_A are shown in Supplemental Material I.B [35]. After some approximations (for details, see Sec. I.C in [35]), the total supercurrent $I_s(\varphi, \Phi)$ can be decoupled into two parts $I_s(\varphi, \Phi) \approx I_{s,c}(\varphi, \Phi) + I_{s,l}(\varphi, \Phi)$, where $I_{s,c}$ and $I_{s,l}$ are defined as the supercurrent arising from the crossed and the local Andreev reflections, respectively, are shown in Fig. 1.

We now study the critical supercurrents when φ varies from 0 to 2π at a fixed Φ, which gives rise to the Fraunhofer pattern. Before looking at the total upper critical supercurrents $I_c(\Phi) = \max_\varphi\{I_s(\varphi, \Phi)\}$, we first study the upper critical currents given by the crossed and the local Andreev reflections, respectively. The upper critical supercurrents $I_{c,c} = \max_\varphi\{I_{s,c}(\varphi, \Phi)\}$, and $I_{c,l} = \max_\varphi\{I_{s,l}(\varphi, \Phi)\}$ are (details derivations can be found in Supplemental Material I.C [35])

$$I_{c,c}(\Phi) \approx \left|I_0 + I_1 \cos\left(\pi\frac{\Phi}{\Phi_0} + \phi'\right)\right|, \qquad (7)$$

$$I_{c,l}(\Phi) \approx \left|-I_2 \cos\left(\pi\frac{\Phi}{\Phi_0} + \phi\right)\right|, \qquad (8)$$

where $I_0 = (2ek_BT/\hbar)\sin^2(\delta kW)\text{sech}\Gamma$, $I_1 = (ek_BT/2\hbar)\sin^2(2\delta kW)\text{sech}^2\Gamma$ with $\Gamma = 2\pi k_B T(d/\hbar v_F + W/\hbar v_s)$ as the ratio between temperature and Thouless energy, $\delta k = \sqrt{\Delta^2 + \mu'^2}/\hbar v_s$ as the Fermi wave vector, $I_2 = (4ek_BT/\hbar)e^{-[(\pi k_B Td/\hbar v_F)+(d/\xi_d)]}$, and the field-independent phase $\phi' = 2\mu d/\hbar v_F + \arctan(2\beta\tan\delta kW)$, $\phi = \mu d/\hbar v_F$.

First of all, one can show that I_0 is always larger than I_1 in $I_{c,c}(\Phi)$, thus the periodicity of $I_{c,c}(\Phi)$ is $2\Phi_0$. This is consistent with previous theoretical findings [23,29]. Importantly, the critical current $I_{c,l}(\Phi)$ possesses a period of Φ_0 Fraunhofer oscillations. Physically, the supercurrents arising from local Andreev reflections mostly enter the supercurrent through top and bottom edges independently, and the interference between these two edges thus acquires a period of Φ_0, which mimics the scenario of the quantum spin Hall Josephson junction [16]. Briefly, the local Andreev reflection induced by the left-right edge coupling originates the Φ_0 periodicity of the Fraunhofer pattern.

To see the crossover from Φ_0 to $2\Phi_0$ periodicity as the junction length increases, we numerically evaluate Eq. (6) without approximations. The calculated Fraunhofer patterns at various lengths with $d/\xi_s = 0.4$, 0.7, 1.2 ($\xi_s = \hbar v_F/\Delta_0$ as superconducting coherence length) are shown in Fig. 2(a). As expected, in the long junction region when $d/\xi_s = 1.2$, the coupling between the left and right CESs is weak and the crossed Andreev
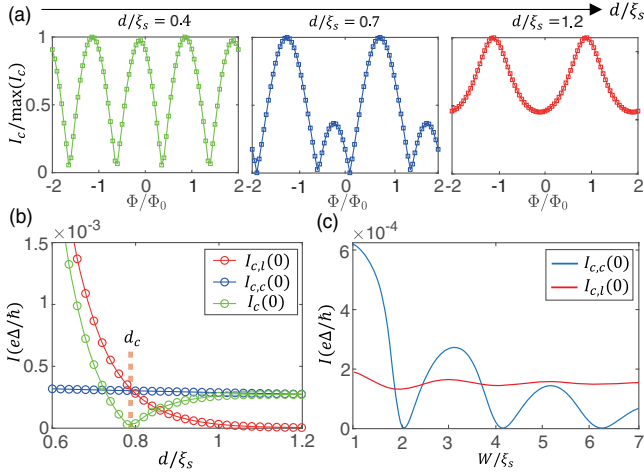
FIG. 2. (a) The crossover from $2\Phi_0$ oscillations to Φ_0 oscillations with the increase of junction length d. (b) The total critical supercurrent I_c, the critical supercurrent from local Andreev reflections $I_{c,c}$, and the critical supercurrent from local Andreev reflections $I_{c,l}$ at zero magnetic flux as a function of d. d_c labels the critical length where $I_c \approx 0$. In (a) and (b), the width of the junction is set as $W/\xi_s = 3$. (c) Junction width dependence of $I_{c,c}$ and $I_{c,l}$ for $d/\xi_s = 0.84$. The width regions are highlighted, where $I_{c,c}$ is larger than $I_{c,l}$. We set the parameters as $v_F = 2$, $\Delta_0 = 0.08$, $\mu = 0.02$, and $\mu' = 0.1$. The coupling strength $g = \Delta_0/5$, which yields $v_s = 1.6$ and $\Delta = \Delta_0/6$. The temperature is $k_B T = 0.05\Delta_0$. To describe the coupling of the edge states, the parameter ξ_d is set to be $0.1\xi_s$, where ξ_s is the superconductor coherent length.

reflection processes dominate. As a result, the $2\Phi_0$-periodic component is dominant. On the other hand, in the short junction case when $d/\xi_s = 0.4$, the local Andreev reflection becomes more significant and the Φ_0-periodic component is dominant.

Figure 2(b) shows the critical currents in the zero magnetic flux ($\Phi = 0$) as a function of junction length d, where $I_{c,c}$ ($I_{c,l}$) only includes crossed (local) Andreev reflection contributions and I_c is the total critical supercurrent. To be more accurate, here $I_{c,c}$ ($I_{c,l}$) is plotted numerically using the full expression from Eq. (6) after separating the total current into these two contributions (see Sec. I.C in [35] for explicit expression). As expected, $I_{c,l}$ decreases more dramatically with the increase of d compared with $I_{c,c}$. Notably, the $I_{c,c}$ and $I_{c,l}$ crossover each other at a critical length d_c, where $I_c \approx 0$. When $d < d_c$, the Φ_0-periodic component can dominate as $I_{c,l} > I_{c,c}$. Figure 2(c) shows the width dependence of the critical current. By fixing $d = 0.84\xi_s$ and increasing W, it can be seen that $I_{c,l}$ is not sensitive to the change of W but $I_{c,c}$ is exponentially suppressed with the width of the junction increases, which is as expected since $I_{c,c}$ arises from the cross Andreev reflections between the top and bottom edge. This is consistent with the recent experiment that the $2\Phi_0$ periodicity was only observed in junctions with small

W [15]. Finally, to further support our theoretical analysis, we adopt a minimal two-band QAHI lattice model in a superconductor/QAHI/superconductor configuration to simulate the Fraunhofer pattern with the lattice Green's function method [39–42]. The lattice model results are fully consistent with the results shown in Fig. 2 of the edge-channel model (for details of the lattice model calculations, see Sec. II.B in [35]). Remarkably, taking the parameters from the two experiments [11,15], we show that the period of oscillations in both experiments can be explained well by our theory (details can be found in Sec. I.E in [35]).

Emergence of MZMs in short junctions—Previously, it was shown that the left-right edge coupling induces the anomalous periodicity of $h/2e$. Here, we demonstrate another important consequence of the left-right edge coupling: the emergence of robust MZMs at the Josephson junction without fine-tuning. The schematic picture of a short Josephson junction with counterpropagating left and right edge modes is depicted in Fig. 3(a). A superconductor-QAHI-superconductor junction lattice model is built in the Supplemental Material II.A [35]. If the left and right edge modes are coupled, we can regard the QAHI weak link as a quasi-1D wire with a single helical channel [7,43,44]. When this helical channel is coupled to a
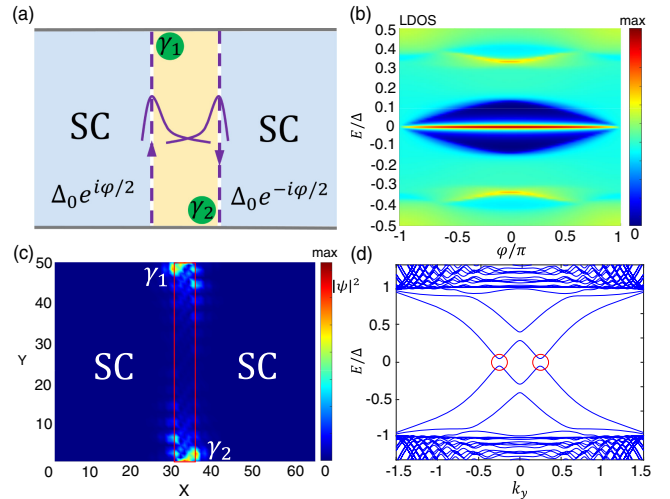
FIG. 3. (a) A short Josephson junction with counterpropagating left and right edge states. When the left and right edge state wave functions overlap (purple lines), MZMs emerge at the ends (labeled as γ_1 and γ_2). (b) The LDOS at one end of the junction versus the phase difference φ. There is a φ-independent MZM. (c) The localized wave function of MZMs at the Josephson junction (the boundary of the junction region is highlighted by a red box). (d) The energy spectrum of superconductor-QAHI-superconductor junction, with the periodic boundary condition along the y direction. The four CAESs emerge in the low-energy states. The energy gaps circled in red are the effective pairing gaps of the states at the Josephson junction. (c) and (d) Correspond to $\varphi = 0$ in (b). See the details in Supplemental Material II.A and II.B [35].

superconductor, MZMs emerge at the two ends of the quasi-1D channel [45–51].

To demonstrate the existence of MZMs in this system, the local density of states (LDOS) at a transverse end of the junction as a function of the Josephson phase difference φ is plotted in Fig. 3(b). The prominent LDOS peak near the zero energy indicates the MZM, which resides inside the pairing gap and is robust against the variation of the phase difference φ [Fig. 3(b)]. Notably, the optimal phase difference is $\varphi = 0$ to maximize the topological superconducting gap. This is in sharp contrast with the previous topological Josephson junction proposals in which the topological regime appears when the phase difference of the junction is near π [52–57]. It is also important to note that the topological superconducting gap protecting the MZM is quite sizable, which is about 10% of the superconducting gap of the superconductors (and it can be further optimized by increasing the coupling between the CAESs from the left and right edges). The wave function of the MZMs is shown in Fig. 3(c), which displays the expected localization behavior at the two ends of the junction.

Figure 3(d) shows the energy spectrum of the Josephson junction. The propagating states inside the pairing gap are the CAESs. When the CAESs from the left and the right edges couple, hybridization gaps emerge, which are highlighted by the red circles. When the hybridization gap is finite, a pair of MZMs emerge at the two ends of the Josephson junction with wave functions depicted in Fig. 3(c). This is the second main result of this Letter. Interestingly, the existence of $h/2e$ Fraunhofer oscillations and the existence of the MZMs originate from the same mechanism in our theory, which is the coupling of the CAESs. Therefore, the appearance of the Φ_0 oscillations in the Fraunhofer pattern may imply the presence of MZMs at the end of chiral Josephson junctions (given that the number of chiral edge states at the junction is odd). Note that there could be other scenarios [12,14], where the Φ_0 periodicity is due to the additional counterpropagating conduction channels introduced by the charge accumulation effect at the weak link boundary (for details see Supplemental Material II.C [35]). Consequently, further experiments are needed to verify the appearance of MZMs.

Conclusion and discussion—In this Letter, we have discovered that an anomalous Φ_0 periodic supercurrent is generated by the coupling of CAESs on opposite edges in CESs-mediated Josephson junctions (chiral Josephson junction). Importantly, the coupling of CAESs is also responsible for the appearance of MZMs at the Josephson junction, as long as the number of CESs at each edge of the weak link is odd. Therefore, by measuring the Φ_0 periodicity of the Fraunhofer pattern, one may identify the parameter regime with MZMs.

Recently, the superconductor-QAHI-superconductor Josephson junction has been realized in the gate-defined Josephson junction in twisted bilayer graphene [58], in which the superconducting states, as well as the QAHI state, can be achieved in a single piece of twisted bilayer graphene sample through electric gating [58–62]. And the model in Fig. 3(a) can also be achieved by depositing superconducting electrodes on moiré transition metal dichalcogenides, where robust QAHI states have been experimentally observed [63–67]. These newly discovered QAHI platforms are promising for observing the $2\Phi_0$ period to Φ_0 period crossover and realizing MZMs.

[1] L. Fu and C. L. Kane, Phys. Rev. Lett. **100**, 096407 (2008).

[2] C. Nayak, S. H. Simon, A. Stern, M. Freedman, and S. D. Sarma, Rev. Mod. Phys. **80**, 1083 (2008).

[3] X.-L. Qi, T. L. Hughes, and S.-C. Zhang, Phys. Rev. B **82**, 184516 (2010).

[4] J. Alicea, Rep. Prog. Phys. **75**, 076501 (2012).

[5] V. Mourik, K. Zuo, S. M. Frolov, S. Plissard, E. P. Bakkers, and L. P. Kouwenhoven, Science **336**, 1003 (2012).

[6] C. Beenakker, Annu. Rev. Condens. Matter Phys. **4**, 113 (2013).

[7] C.-Z. Chen, Y.-M. Xie, J. Liu, P. A. Lee, and K. T. Law, Phys. Rev. B **97**, 104504 (2018).

[8] A. Yazdani, F. von Oppen, B. I. Halperin, and A. Yacoby, Science **380**, eade0850 (2023).

[9] M. Ma and A. Y. Zyuzin, Europhys. Lett. **21**, 941 (1993).

[10] V. E. Calado, S. Goswami, G. Nanda, M. Diez, A. R. Akhmerov, K. Watanabe, T. Taniguchi, T. M. Klapwijk, and L. M. Vandersypen, Nat. Nanotechnol. **10**, 761 (2015).

[11] F. Amet, C. T. Ke, I. V. Borzenets, J. Wang, K. Watanabe, T. Taniguchi, R. S. Deacon, M. Yamamoto, Y. Bomze, S. Tarucha et al., Science **352**, 966 (2016).

[12] A. W. Draelos, M. T. Wei, A. Seredinski, C. T. Ke, Y. Mehta, R. Chamberlain, K. Watanabe, T. Taniguchi, M. Yamamoto, S. Tarucha et al., J. Low Temp. Phys. **191**, 288 (2018).

[13] S. Guiducci, M. Carrega, G. Biasiol, L. Sorba, F. Beltram, and S. Heun, Phys. Status Solidi RRL **13**, 1800222 (2019).

[14] A. Seredinski, A. W. Draelos, E. G. Arnault, M.-T. Wei, H. Li, T. Fleming, K. Watanabe, T. Taniguchi, F. Amet, and G. Finkelstein, Sci. Adv. **5**, eaaw8693 (2019).

[15] H. Vignaud, D. Perconte, W. Yang, B. Kousar, E. Wagner, F. Gay, K. Watanabe, T. Taniguchi, H. Courtois, Z. Han et al., Nature (London) **624**, 545 (2023).

[16] S. Hart, H. Ren, T. Wagner, P. Leubner, M. Mühlbauer, C. Brüne, H. Buhmann, L. W. Molenkamp, and A. Yacoby, Nat. Phys. **10**, 638 (2014).

[17] F. Schindler, Z. Wang, M. G. Vergniory, A. M. Cook, A. Murani, S. Sengupta, A. Y. Kasumov, R. Deblock, S. Jeon, I. Drozdov *et al.*, Nat. Phys. **14**, 918 (2018).

[18] Y.-B. Choi, Y. Xie, C.-Z. Chen, J. Park, S.-B. Song, J. Yoon, B. J. Kim, T. Taniguchi, K. Watanabe, J. Kim *et al.*, Nat. Mater. **19**, 974 (2020).

[19] A. Bernard, Y. Peng, A. Kasumov, R. Deblock, M. Ferrier, F. Fortuna, V. Volkov, Y. A. Kasumov, Y. Oreg, F. von Oppen *et al.*, Nat. Phys. **19**, 358 (2023).

[20] B. Baxevanis, V. Ostroukh, and C. Beenakker, Phys. Rev. B **91**, 041409(R) (2015).

[21] F. K. De Vries, T. Timmerman, V. P. Ostroukh, J. Van Veen, A. J. Beukman, F. Qu, M. Wimmer, B.-M. Nguyen, A. A. Kiselev, W. Yi *et al.*, Phys. Rev. Lett. **120**, 047702 (2018).

[22] L. Vigliotti, A. Calzona, B. Trauzettel, M. Sassetti, and N. T. Ziani, New J. Phys. **24**, 053017 (2022).

[23] J. A. M. Van Ostaay, A. R. Akhmerov, and C. W. J. Beenakker, Phys. Rev. B **83**, 195441 (2011).

[24] R. Nakai, K. Nomura, and Y. Tanaka, Phys. Rev. B **103**, 184509 (2021).

[25] Y. Tang, C. Knapp, and J. Alicea, Phys. Rev. B **106**, 245411 (2022).

[26] V. D. Kurilovich, Z. M. Raines, and L. I. Glazman, Nat. Commun. **14**, 2237 (2023).

[27] M. Stone and Y. Lin, Phys. Rev. B **83**, 224501 (2011).

[28] J. Liu, H. Liu, J. Song, Q.-F. Sun, and X. C. Xie, Phys. Rev. B **96**, 045401 (2017).

[29] Y. Alavirad, J. Lee, Z.-X. Lin, and J. D. Sau, Phys. Rev. B **98**, 214504 (2018).

[30] F. Dominguez, E. Novik, and P. Recher, Phys. Rev. Res. **6**, 023304 (2024).

[31] C. W. J. Beenakker, Phys. Rev. Lett. **67**, 3836 (1991).

[32] G.-H. Lee, K.-F. Huang, D. K. Efetov, D. S. Wei, S. Hart, T. Taniguchi, K. Watanabe, A. Yacoby, and P. Kim, Nat. Phys. **13**, 693 (2017).

[33] L. Zhao, E. G. Arnault, A. Bondarev, A. Seredinski, T. F. Larson, A. W. Draelos, H. Li, K. Watanabe, T. Taniguchi, F. Amet *et al.*, Nat. Phys. **16**, 862 (2020).

[34] P. Brouwer and C. Beenakker, Chaos, Solitons Fractals **8**, 1249 (1997).

[35] See Supplemental Material at http://link.aps.org/supplemental/10.1103/PhysRevLett.133.056601 for the analytical calculations from the scattering matrix method, the numerical simulations from the recursive Green's function method in terms of the tight-binding model of QAHI, and some discussions on the effect of the gate-induced extra counterpropagating channels on the weak link edges, which includes Refs. [36–38].

[36] X.-L. Qi, Y.-S. Wu, and S.-C. Zhang, Phys. Rev. B **74**, 085308 (2006).

[37] Y.-T. Zhang, Z. Hou, X. C. Xie, and Q.-F. Sun, Phys. Rev. B **95**, 245433 (2017).

[38] Y.-H. Li and R. Cheng, Phys. Rev. Res. **4**, 033227 (2022).

[39] A. Furusaki, Physica (Amsterdam) **203B**, 214 (1994).

[40] T. Ando, Phys. Rev. B **44**, 8017 (1991).

[41] Y. Asano, Phys. Rev. B **63**, 052512 (2001).

[42] Y. Asano, Y. Tanaka, M. Sigrist, and S. Kashiwaya, Phys. Rev. B **67**, 184505 (2003).

[43] Y.-M. Xie, X.-J. Gao, T.-K. Ng, and K. Law, arXiv:2012.15523.

[44] K. T. Law, X. Yingming, and G. Xuejian, Creating Majorana zero modes in quantum anomalous Hall insulator/ superconductor heterostructures, Us Patent App. 17/672, 434 (2022).

[45] A. Y. Kitaev, Phys. Usp. **44**, 131 (2001).

[46] Y. Oreg, G. Refael, and F. Von Oppen, Phys. Rev. Lett. **105**, 177002 (2010).

[47] J. D. Sau, R. M. Lutchyn, S. Tewari, and S. D. Sarma, Phys. Rev. Lett. **104**, 040502 (2010).

[48] R. M. Lutchyn, J. D. Sau, and S. D. Sarma, Phys. Rev. Lett. **105**, 077001 (2010).

[49] R. M. Lutchyn, T. D. Stanescu, and S. D. Sarma, Phys. Rev. Lett. **106**, 127001 (2011).

[50] T.-P. Choy, J. M. Edge, A. R. Akhmerov, and C. W. J. Beenakker, Phys. Rev. B **84**, 195442 (2011).

[51] J. Klinovaja, P. Stano, A. Yazdani, and D. Loss, Phys. Rev. Lett. **111**, 186805 (2013).

[52] F. Pientka, A. Keselman, E. Berg, A. Yacoby, A. Stern, and B. I. Halperin, Phys. Rev. X **7**, 021032 (2017).

[53] M. Hell, M. Leijnse, and K. Flensberg, Phys. Rev. Lett. **118**, 107701 (2017).

[54] C. T. Ke, C. M. Moehle, F. K. de Vries, C. Thomas, S. Metti, C. R. Guinn, R. Kallaher, M. Lodari, G. Scappucci, T. Wang *et al.*, Nat. Commun. **10**, 3764 (2019).

[55] A. Fornieri, A. M. Whiticar, F. Setiawan, E. Portolés, A. C. Drachmann, A. Keselman, S. Gronin, C. Thomas, T. Wang, R. Kallaher *et al.*, Nature (London) **569**, 89 (2019).

[56] H. Ren, F. Pientka, S. Hart, A. T. Pierce, M. Kosowsky, L. Lunczer, R. Schlereth, B. Scharf, E. M. Hankiewicz, L. W. Molenkamp *et al.*, Nature (London) **569**, 93 (2019).

[57] Y.-M. Xie, E. Lantagne-Hurtubise, A. F. Young, S. Nadj-Perge, and J. Alicea, Phys. Rev. Lett. **131**, 146601 (2023).

[58] J. Díez-Mérida, A. Díez-Carlón, S. Yang, Y.-M. Xie, X.-J. Gao, J. Senior, K. Watanabe, T. Taniguchi, X. Lu, A. P. Higginbotham *et al.*, Nat. Commun. **14**, 2396 (2023).

[59] A. L. Sharpe, E. J. Fox, A. W. Barnard, J. Finney, K. Watanabe, T. Taniguchi, M. Kastner, and D. Goldhaber-Gordon, Science **365**, 605 (2019).

[60] M. Serlin, C. Tschirhart, H. Polshyn, Y. Zhang, J. Zhu, K. Watanabe, T. Taniguchi, L. Balents, and A. Young, Science **367**, 900 (2020).

[61] Y.-M. Xie, D. K. Efetov, and K. T. Law, Phys. Rev. Res. **5**, 023029 (2023).

[62] J.-X. Hu, Z.-T. Sun, Y.-M. Xie, and K. T. Law, Phys. Rev. Lett. **130**, 266003 (2023).

[63] T. Li, S. Jiang, B. Shen, Y. Zhang, L. Li, Z. Tao, T. Devakul, K. Watanabe, T. Taniguchi, L. Fu *et al.*, Nature (London) **600**, 641 (2021).

[64] J. Cai, E. Anderson, C. Wang, X. Zhang, X. Liu, W. Holtzmann, Y. Zhang, F. Fan, T. Taniguchi, K. Watanabe *et al.*, Nature (London) **622**, 63 (2023).

[65] Y. Zeng, Z. Xia, K. Kang, J. Zhu, P. Knüppel, C. Vaswani, K. Watanabe, T. Taniguchi, K. F. Mak, and J. Shan, Nature (London) **622**, 69 (2023).

[66] H. Park, J. Cai, E. Anderson, Y. Zhang, J. Zhu, X. Liu, C. Wang, W. Holtzmann, C. Hu, Z. Liu *et al.*, Nature (London) **622**, 74 (2023).

[67] F. Xu, Z. Sun, T. Jia, C. Liu, C. Xu, C. Li, Y. Gu, K. Watanabe, T. Taniguchi, B. Tong *et al.*, Phys. Rev. X **13**, 031037 (2023).